Study of plasma confinement by magnetic fields in Hall thrusters using Quasi-Neutral PIC modeling

IEPC-2011-238

Presented at the 32nd International Electric Propulsion Conference,
Wiesbaden, Germany
September 11–15, 2011

Jan Miedzik* and Serge Barral†
Institute of Plasma Physics and Laser Microfusion, 01-497 Warsaw, Poland

and

Stéphan Zurbach‡
Snecma, Safran Group, 27208 Vernon, France

Abstract: A 1D3V quasi-neutral particle-in-cell model based on the guiding center approximation for electron motion with unmagnetized ions is employed to study the influence of the angle between magnetic field lines and confining walls on plasma properties in the discharge channel of a Hall thruster. The model accounts, among others, for the influence of magnetic field gradients on plasma confinement, for temperature anisotropy and for secondary electron emission from the walls. Simulations reveal that for angles between the magnetic field and the normal to the wall less than 40°, magnetic field orientation has very little effect on plasma/wall interactions. As the magnetic field orientation becomes more parallel to the walls, however, orientation becomes more important since electrons more frequently intercept the sheath edge at grazing incidence. For ion-focusing magnetic topologies, electrons intercepting at grazing angles have an energy close to the maximum energy during cyclotron rotation, hence an increase of the deposited energy and electron secondary emission. In contrast, for ion-defocusing topologies, the energy deposited and secondary electron emission are lower than at normal incidence.

*PhD student, Division of Magnetised Plasma, jan.miedzik@ipplm.pl.
†Assistant Professor, Division of Magnetised Plasma, serge.barral@ipplm.pl.
‡R & D Engineer, Space Engines Division, stephan.zurbach@snecma.fr.

Nomenclature

$\mathbf{B}$, B = magnetic field (vector, magnitude)

e = absolute electron charge

$\mathscr{E}_0$ = total electron energy

$\mathscr{E}_\parallel$ = electron energy along $\mathbf{B}$

$\mathscr{E}_\perp$ = electron energy perpendicular to $\mathbf{B}$

$E_\parallel$ = electric field along $\mathbf{B}$

$\hat{\mathscr{E}}_{ts}$ = SEE model parameter

f_v = electron velocity distribution function

f_ε = electron energy distribution function

j_{ew} = current density of electrons impinging walls

j_{iw} = current density of ions impinging walls

m_e = electron mass

m_i = ion mass

n_n = density of neutrals

$N_{n,e,i}$ = number of neutrals, electrons, ions

P_n = probability of emission of n secondary electrons

$P_{n,ts}$ = probability of emission of n true secondary electrons

R = random number

T_e = total electron temperature

$T_{e\parallel}$ = electron temperature along $\mathbf{B}$

$T_{e\perp}$ = electron temperature perpendicular to $\mathbf{B}$

$T_{e\top}$ = electron temperature perpendicular to the wall

$v_\perp$ = electron velocity in the drifting frame

v_i = ions velocity along $\mathbf{B}$

w_e = SEE model parameter

α = angle between the normal to the wall and $\mathbf{B}$

δ = SEE yield

δ_{e0} = extrapolated elastic backscattering yield at zero energy

δ_e = elastic backscattering electron emission yield

δ_{max} = maximum theoretical value of SEE yield

δ_r = inelastic backscattering electron emission yield

δ_{ts} = true SEE yield

$\hat{\delta}_{ts}$ = maximum true SEE yield

ζ = field line curvilinear coordinate

κ = Boltzmann constant

μ = electron magnetic moment, $\mu \equiv \frac{1}{2} m_e v_\perp^2 / B$

$\Phi_{bi,o}$ = potential barrier of the wall sheath

$\Phi_{wi,o}$ = well potential for secondary electrons emitted from the wall

I. Introduction

Although the intricacy of Hall thruster physics impedes the predictive ability of numerical models, the parametric exploration of such models can often offer very valuable insights that would be impossible to obtain experimentally in a cost-effective manner. In particular, the influence of the magnetic lens, has recently been at the focus of several numerical modeling studies.

Magnetic mirror effects have been investigated by means of different plasma description. Keidar and Boyd,[1] using a fluid description, have shown that the *B*-field gradient affects plasma potential and the presheath structure. Later studies by Choi *et al.*[2] with a hybrid model, have shown a very good agreement with experimental data when both the magnetic field and the departure from the ideal Boltzmann relation are accounted for.

The influence of the angle between *B*-field lines and the wall for a fully magnetized plasma was studied from a theoretical perspective by Ahedo and Carralero.[3] Keidar and Beilis[4] have in turn found that the potential drop across the sheath tends to increase with the angle between the normal to the wall and the magnetic field if an angle-dependent secondary electron emission yield is accounted for.

The ability of quasineutral kinetic/guiding center modeling[5,6] to account for magnetic mirror effects makes it particularly suitable for the study of magnetic plasma confinement in Hall thrusters, currently a very active area of research for both annular-type and cylindrical thrusters. In a previous work by the authors,[7] the importance of magnetic gradients in the presence of electron temperature anisotropy has been underlined, demonstrating the impossibility to properly account for magnetic lenses effect if electron temperature isotropy is postulated and the classical Boltzmann relation is used. In this work, the physical description of the model has been improved in important ways by including ion dynamics (whereas in the former model[7] plasma density was imposed *a priori*), a detailed secondary electron emission model and the incidence angle of *B*-field lines with the walls.

II. Physical and numerical model

A. Particle motion and electric field

Details of the electrons motion model and of the calculation of the electric field have been presented earlier in Ref. 7. Electrons are treated as guiding center (GC) particles, and their equation of motion is integrated using the 2nd order SIMP method described by Fuchs and Gunn.[8] The electric field is calculated self-consistently from the electron momentum equation, using the modified momentum equation suggested by

Lampe *et al.*[6]

Compared to our previous model where ions formed a static background, the motion of ions is now resolved self-consistently. Since the model is 1D, ions are submitted to the electric field parallel to **B** only, and the effect of the electric field perpendicular to **B** is disregarded. Because of the relatively low magnetic field strength, the magnetic component of the Lorentz force acting on ions is neglected and the equation of motion is reduced to

$$\frac{dv_i}{dt} = \frac{e}{m_i} E_{\parallel}. \tag{1}$$

Integration of ion motion is performed with Euler scheme (1$^{\text{st}}$ order).

B. Tilted magnetic field lines

1. *Problem statement*

A notable improvement of the electron-wall interaction model is that it can now account for magnetic lines that are not perpendicular to the walls. An important consequence of magnetic lines tilted with respect to the normal to the wall is that the magnetic momentum $\mu \equiv v_\perp^2/2B$ changes even after reflection on the Debye sheath (assumed infinitely thin), while in the case of perpendicular field lines it could only change after a diffusive collision with the wall surface. It is therefore necessary to recompute the electron kinetic state at each reflection on the sheath. Since reflection on the sheath is a very frequent event, the evaluation of the new kinetic state must be done in the most efficient manner.

The electron kinetic state after reflection on the sheath is, however, dependent on the kinetic state just prior to reflection and in particular on the electron gyrophase upon impact. The gyrophase is not explicitly resolved in a guiding center model, but since the electron cyclotron frequency is much larger than the characteristic collision frequency, it is in general reasonable to assume that the correlation of gyrophases between subsequent collisions is lost. In the case where **B** is perpendicular to the walls, one can thus assume that the electron gyrophase upon interception with the wall or upon reflection on the sheath is equiprobably distributed in the $[0, 2\pi]$ interval. When field lines are tilted, however, the probability distribution becomes non-trivial due to the fact that electrons intercept the wall more often on the side of the magnetic flux tube that lies alongside the wall (see Fig. 1). In such case, a Kepler-type equation,

$$\Psi = \phi - \left(\frac{v_\perp}{v_z}\tan\alpha\right)\sin\phi \tag{2}$$

can be solved to determine the gyrophase ϕ of the first interception with the wall (that is, the smallest ϕ that is solution of the above equation). This equation takes as input a random reference gyrophase Ψ in an arbitrary section of the magnetic tube that uniquely defines the angular shift of the helical trajectory, as well as the angle α between the field line and the normal to the wall. The reference gyrophase Ψ is generated from an equiprobable distribution in the $[0, 2\pi]$ interval. Unlike the canonical Kepler's equation, the "eccentricity"

$$\mathsf{e} \equiv \frac{v_\perp}{v_z}\tan\alpha, \tag{3}$$

can be equal to or greater than 1. Unfortunately, Kepler's equation is notoriously difficult to solve for $\mathsf{e} \approx 1$.

Worse yet, for $e > 1$ it may have several roots and the convergence of fast root-finding methods is no longer guaranteed. In practice, Eq. (2) would thus need to be solved by the robust but relatively slow bisection method, which would have a large impact on the overall computational cost of the simulation.

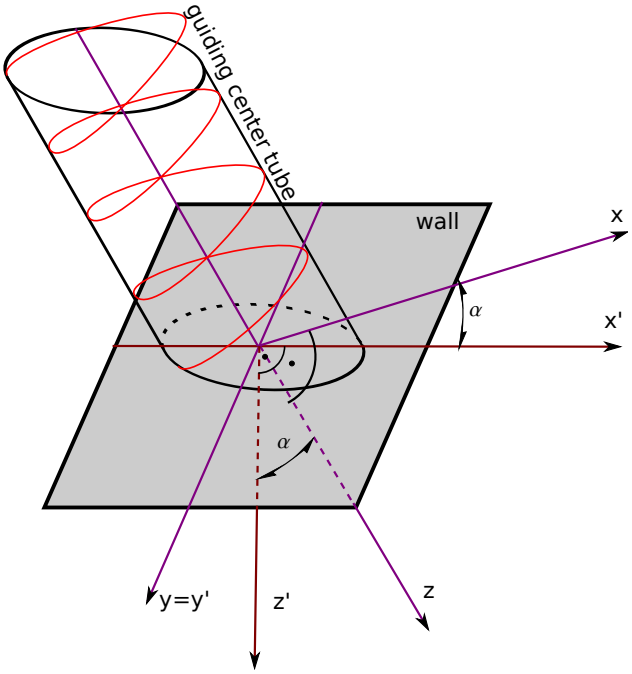

Figure 1: Interception of electrons on a magnetic flux tube non-normal to the wall.

.

2. *A fast probabilistic method*

Because collisions with the sheath are very frequent, a more efficient method than the bisection root-finding method is required. It is indeed possible to avoid altogether the resolution of Eq. (2) by determining directly the probability distribution of ϕ analytically, so that random ϕ values can be generated without need for an iterative solver.

CASE $0 \leq e \leq 1$ In this case, the probability distribution $\mathscr{P}_\phi$ of ϕ in the $[0, 2\pi]$ interval can be determined using the property:

$$\int_0^\phi \mathscr{P}_\phi d\phi^* = \int_0^\Psi \mathscr{P}_\Psi d\Psi^*. \tag{4}$$

Since the angular position of the helical electron trajectory is considered equiprobable in the $[0, 2\pi]$ interval, then the probability for Ψ is simply

$$\mathscr{P}_\Psi = \frac{1}{2\pi} \qquad \Psi \in [0, 2\pi], \tag{5}$$

hence, by virtue of Eq. (2),

$$\int_0^\Psi \mathscr{P}_\Psi d\Psi^* = \frac{\Psi}{2\pi} = \frac{1}{2\pi}(\phi - e\sin\phi). \tag{6}$$

Having Eq. (4) in mind, the above equation can be differentiated with respect to ϕ to obtain,

$$\mathscr{P}_\phi = \frac{1}{2\pi}\left(1 - \mathsf{e}\cos\phi\right) \qquad \phi \in [0, 2\pi]\,. \tag{7}$$

CASE $\mathsf{e} > 1$ This case is much more intricate, since ϕ is now constrained to a subinterval of $[0, 2\pi]$ which is yet to be determined. Indeed, for $\mathsf{e} > 1$, the helical trajectory crosses the wall plane for several values of ϕ and one must therefore retain only the phase that correspond to the first interception. For $\phi \in [0, 2\pi]$, the first possible value of ϕ at interception is that for which the helical trajectory was exactly tangent to the wall at an earlier point $-\frac{\pi}{2} < \phi_T < 0$. The gyrophase ϕ_T at which such trajectory is tangent to the wall is easily determined by differentiating Eq. (2) with respect to ϕ, which raises:

$$\phi_T = -\arccos\left(\frac{1}{\mathsf{e}}\right). \tag{8}$$

This can be reinjected into Eq. (2) to obtain the corresponding Ψ_T:

$$\Psi_T = -\arccos\left(\frac{1}{\mathsf{e}}\right) + \sqrt{\mathsf{e}^2 - 1}. \tag{9}$$

Solving Kepler's equation with $\Psi = \Psi_T$,

$$\Psi_T\left(\mathsf{e}\right) = \phi_0 - \mathsf{e}\sin\phi_0 \tag{10}$$

one can obtain the smallest possible value ϕ_0 within $[0, 2\pi]$ at which a trajectory can intercept the wall for the first time. This solution is obviously only dependent on e,

$$\phi_0 = \phi_0\left(\mathsf{e}\right), \tag{11}$$

but cannot be put in a close analytical form. We shall discuss later how this issue can be overcome.

The largest possible value of ϕ in the $[\phi_0, 2\pi]$ interval is in turn the one for which the trajectory becomes again tangent to the wall, *i.e.*

$$\phi_1 = \phi_T + 2\pi = 2\pi - \arccos\left(\frac{1}{\mathsf{e}}\right) \tag{12}$$

The probability distribution of ϕ for $\mathsf{e} > 1$ is thus

$$\mathscr{P}_\phi = \begin{cases} \dfrac{1 - \mathsf{e}\cos\phi}{2\pi} & \phi \in [\phi_0\left(\mathsf{e}\right), \phi_1\left(\mathsf{e}\right)] \\ 0 & \phi \in [0, \phi_0\left(\mathsf{e}\right)[\cup]\phi_1\left(\mathsf{e}\right), 2\pi] \end{cases} \tag{13}$$

CASE $\mathsf{e} < 0$ This case can be reduced to the previous two cases by noting that when $\mathsf{e} < 0$, one can write

$$\Psi + \pi = (\phi + \pi) - |\mathsf{e}|\sin\left(\phi + \pi\right). \tag{14}$$

It is therefore enough to solve for $|\mathsf{e}|$ and subtract π from the value ϕ ultimately obtained.

3. Numerical method

A simple method for random number generation is the rejection method. Let us assume for now that the bounds of the interval $[\phi_0, \phi_1]$ in which the probability density $\mathscr{P}_\phi$ is non-zero can be computed explicitly (note that for $\mathsf{e} < 1$ the interval is simply $[0, 2\pi]$).

In its simplest variant, the rejection method involves finding an upper bound $\hat{p}$ of $\mathscr{P}_\phi$, which in our case can be trivially computed as,

$$\hat{p} = \begin{cases} \dfrac{1+\mathsf{e}}{2\pi} & \phi_0 \leq \pi \\ \dfrac{1-\mathsf{e}\cos\phi_0}{2\pi} & \phi_0 > \pi \end{cases}. \tag{15}$$

A set of two random numbers $\phi \in [\phi_0, \phi_1]$ and $p \in [0, \hat{p}]$ is then generated using uniform probability distributions. If $p < \mathscr{P}_\phi(\phi)$, then the number ϕ is accepted. Otherwise, subsequent pairs of (ϕ, p) are generated until the condition is fulfilled. Obviously, the number of discarded results is minimized when the area $\int_{\phi_0}^{\phi_1} \mathscr{P}_\phi d\phi$ is large compared to $\hat{p}(\phi_1 - \phi_0)$. In our case, it can be shown that the area ratio is always 50% or greater, meaning that on average less than 2 trials are required to obtain an acceptable value of ϕ.

In practice, however, only $\phi_1(\mathsf{e})$ can be expressed in an explicit analytical form [see Eq. (12)] while $\phi_0(\mathsf{e})$ cannot. One possibility would be to solve once for all Eq. (10) and approximate ϕ_0 by numerical interpolation using piecewise linear or cubic spline functions. We shall prefer, however, another method that does not involve any approximation and is similarly fast. The key to this method is to find a lower bound $\check{\phi}_0(\mathsf{e}) \leq \phi_0(\mathsf{e})$ that can be explicitly expressed and to apply the rejection method over the extended interval $\left[\check{\phi}_0, \phi_1\right]$, discarding a posteriori results that fall within the range $\left[\check{\phi}_0, \phi_0\right]$ by testing whether the condition

$$\phi - \mathsf{e}\sin\phi > \Psi_T, \tag{16}$$

is satisfied.

Seeking for a lower bound $\check{\phi}_0$, it is very convenient to substitute $\mathsf{e} \in [1, \infty[$ by

$$a \equiv \frac{1}{\pi}\arccos\left(\frac{2}{\mathsf{e}} - 1\right) \qquad a \in [0, 1], \tag{17}$$

because function $\phi_0(a)$ happens to exhibit a very good linearity over the whole $[0, 1]$ range. This mapping would also have been very convenient had we opted for a numerical interpolation of the numerical solution of Eq. (10). It is now possible to provide a lower bound $\check{\phi}_0(a) \leq \phi_0(a)$ in terms of a cubic Hermite spline,

$$\check{\phi}_0 \equiv \pi a\left[\sqrt{2}\left(a^2 - 2a + 1\right) + \left(-3a^2 + \frac{9}{2}a\right) + \sqrt{\pi}\left(a^2 - a\right)\right] \tag{18}$$

which matches ϕ_0 and $d\phi_0/da$ exactly at the $a = 0$ and $a = 1$ and remains very close to ϕ_0 everywhere ($0 \leq \phi_0 - \check{\phi}_0 < 0.032$). Owing to the very small difference between ϕ_0 and $\check{\phi}_0$, very few numbers fall in the range $\left[\check{\phi}_0, \phi_0\right]$ and the test condition (16) is thus nearly systematically fulfilled. The impact on the number of trials required to obtain ϕ is therefore negligible (in fact, it can be proved that the worse case is still strictly equal to 2 trials per ϕ on average).

The numerical algorithm for the determination of ϕ in all cases is summarized in Algorithm 1

Algorithm 1 Calculate gyrophase ϕ upon electron reflection on the sheath or upon wall impact for tilted magnetic field lines.
Note: function rand(x_1, x_2) returns a random real number between x_1 and x_2 with a uniform probability density.

if $|\mathsf{e}| < 1$ **then**
  $\hat{p} \leftarrow (1 + |\mathsf{e}|)/2\pi$
  repeat
    $\phi \leftarrow \text{rand}(0, 2\pi)$
    $p \leftarrow \text{rand}(0, \hat{p})$
  until $p < (1 - |\mathsf{e}| \cos\phi)/2\pi$
else
  $a \leftarrow \arccos(2/|\mathsf{e}| - 1)/\pi$
  $\check{\phi}_0 \leftarrow \pi a \left[\sqrt{2}\left(a^2 - 2a + 1\right) + \left(-3a^2 + \frac{9}{2}a\right) + \sqrt{\pi}\left(a^2 - a\right)\right]$
  $\phi_1 \leftarrow 2\pi - \arccos(1/|\mathsf{e}|)$
  if $\check{\phi}_0 \leq \pi$ **then**
    $\hat{p} \leftarrow (1 + |\mathsf{e}|)/2\pi$
  else
    $\hat{p} \leftarrow \left(1 - |\mathsf{e}| \cos\check{\phi}_0\right)/2\pi$
  end if
  repeat
    $\phi \leftarrow \text{rand}(\check{\phi}_0, \phi_1)$
    $p \leftarrow \text{rand}(0, \hat{p})$
  until $p < (1 - |\mathsf{e}| \cos\phi)/2\pi$ **and** $\phi - |\mathsf{e}| \sin\phi > -\arccos(1/|\mathsf{e}|) + \sqrt{\mathsf{e}^2 - 1}$
end if
if $\mathsf{e} < 0$ **then**
  $\phi \leftarrow \phi - \pi$
end if
return ϕ

C. Secondary electron emission (SEE) model

The secondary electron yield noticeably impacts the operating conditions of Hall thrusters,[9–11] mainly via the wall potential and temperature of electrons re-entering the plasma. The decrease in SEE causes an increase of the wall potential and thus a decrease of the number of electrons which can overcome the wall potential and undergo collisions with the wall. Likewise, the electron temperature inside the channel changes depending on the boundary conditions, which influences in turn the ionization rate.

For the sake of simplicity, and in the absence of a widely accepted theory of SEE at low energy, the total SEE yield is assumed to behave linearly in the energy range $0-100$eV, which appears consistent with the limited experimental data available for ceramics of interest in Hall thrusters.[12–14]These experimental data do not distinguish, however, true secondary electrons from elastically and inelastically backscattered electrons. The scarcity of experimental data, especially for insulators, make it necessary to estimate the respective emitted electron fractions using purely phenomenological arguments.

Such a phenomenological model was proposed by Furman and Pivi,[15] and used later by Taccogna *et al.*[16] It is necessary to underline, however, that this model is exclusively based on experimental data for electrical conductors. Besides, the very large number of free parameters of this model and very small number of relevant experimental references makes fitting to experiments somewhat illusory. The next subsection describes simplifications that have been made to the model of Furman and Pivi in order to obtain a more manageable number of free parameters.

1. General assumptions

The model of secondary electron emission is based on the one developed by Furman and Pivi,[15] with some simplifications to be described later on. The guiding phenomenological principles of the model are the following:

- the total energy of all secondary electrons cannot be higher than the energy of the primary electron,
- in the absence of specific experimental data concerning the angle dependence of SEE and having in consideration the porosity of ceramics used in Hall thrusters, the angular dependence of the SEE yield on primary electron velocity is neglected,
- the angular distribution of inelastically backscattered and true secondary electrons follows a cosine law[17]
- the energy of elastically backscattered electrons remains unchanged after collision; the energy of inelastically backscattered electrons is sampled from a Maxwellian flux distribution truncated at the energy of the primary electron (a constant temperature of 5eV was assumed in later calculations)
- the *total* energy of all secondary electrons is sampled uniformly in the interval $[0, \mathscr{E}_0]$ where $\mathscr{E}_0$ is the primary electron energy.

Elastic reflection

Since the penetration depth of very energetic electrons is usually large, it seems reasonable to assume that the elastic backscattering yield vanishes at infinitely high electron energy, $\delta_{1,e}(\infty) = 0$. The original elastic backscattering yield formula of Furman and Pivi was accordingly simplified as

$$\delta_e(\mathscr{E}_0) = \delta_{e0} \exp(-\frac{\mathscr{E}_0}{w_e}). \tag{19}$$

Inelastic backscattering

Since the inelastic backscattering yield formula of Furman and Pivi with the parameters assumed by Taccogna[16] gives a fairly constant value of δ_r, this formula was simply reduced to

$$\delta_r = \text{const.} \tag{20}$$

True secondary

The original formula proposed by Furman and Pivi for the true secondary electron yield was kept unchanged, that is:

$$\delta_{ts}(\mathscr{E}_0) = \hat{\delta}_{ts} D\left(\mathscr{E}_0 / \hat{\mathscr{E}}_{ts}\right), \tag{21}$$

where

$$D(x) = \frac{sx}{s-1+x^s},$$

with $s > 1$ an adjustable parameter. This formula is consistent with the fact that δ_{ts} presents a maximum $\hat{\delta}_{ts}$ at an energy $\hat{\mathscr{E}}_{ts}$.

Emission probabilities

All components of the SEE having been defined, it is necessary to define the probability for emitting n true secondary electrons, $P_{n,ts}$. As suggested by Furman and Pivi, a Poisson distribution is chosen to calculate the probability of creation n true secondary electrons

$$P_{n,ts} = \frac{\delta_{ts}^n}{n!} e^{-\delta_{ts}}, \quad n \geq 0.,$$

It is important to underline that, in order to ensure that the total probability of absorption and of unitary electron emission fall within the physical range $[0,1]$, the probability $P_{n,ts}$ must be calculated only for those primary electrons which are known not to be backscattered (*i.e.* for a statistical fraction $1 - \delta_e - \delta_r$ of the incident electron flux).

The overall probabilities for the emission of n electrons —irrespective of their nature— are thus[15]

$$\begin{aligned} P_0 &= (1-\delta_e-\delta_r)\,P_{0,ts} \\ P_1 &= (1-\delta_e-\delta_r)\,P_{1,ts} + \delta_e + \delta_r \\ P_n &= (1-\delta_e-\delta_r)\,P_{n,ts} \qquad n \geq 2 \end{aligned}$$

where P_0 is the probability for a colliding electron to be absorbed, P_1 is the probability for a true secondary or backscattered electron to be emitted, and P_n is the probability for n electrons to be emitted.

Since $\sum P_n = 1$, a numerically efficient method that avoids the explicit computation of the entire sequence $\{P_n\}$ consist in sampling a random number R uniformly in the interval $[0,1]$ and to calculate the first terms of sequence $\{P_n\}$ until the sum of all such terms becomes greater than R. The last value of n calculated is the number of emitted electrons (see Alg. 2).

Energy of true secondary electrons

Furman and Pivi have assumed an ad-hoc formula for the spectrum of secondary electrons, intended to fit experimental data for metals. Since virtually no experimental data exist for ceramics in the energy of interest for Hall thrusters, the model was simplified by assuming that the total energy $\mathscr{E}_s$ of all secondary electrons is uniformly distributed in the interval $[0,\mathscr{E}_0]$ where $\mathscr{E}_0$ is the energy of the primary electron.

The problem is trivial in the case of a single secondary electron; for $n > 1$ true secondary electrons, however, it is necessary to distribute energy $\mathscr{E}_0$ over all n secondary electrons. Taking some inspiration from the "uncorrelated" distribution of Furman and Pivi, we shall assume that the velocities of secondary electrons are the coordinates of points that are uniformly distributed over the surface of a n-dimensional hypersphere of radius $v_s \equiv 2/m_e\sqrt{\mathscr{E}_s}$. This ensures that $\sum v_i^2 = v_s^2$ and therefore that the sum of all energies is, by construction, equal to $\mathscr{E}_s$.

The trigonometrical method used by Furman and Pivi to compute such coordinates is rather complex and error-prone. A much simpler but formally equivalent method is to project on the hypersphere a n-dimensional vector $\hat{\mathbf{v}} = \{\hat{v}_1, \hat{v}_2, \ldots \hat{v}_n\}$ which coordinates are each independently given by a standard normal distribution. Noting that the probability density associated with $\hat{\mathbf{v}}$ is

$$\prod_{i-1}^{n} \exp\left(-\frac{1}{2}\hat{v}_i^2\right) = \exp\left(-\frac{1}{2}\sum_{i-1}^{n}\hat{v}_i^2\right) = \exp\left(-\frac{1}{2}\left\|\hat{\mathbf{v}}\right\|^2\right),$$

it becomes obvious that this statistical distribution is spherically symmetric in the n-dimensional velocity space and that its projection on the hypersphere of radius v_s is indeed uniform over the hypersphere. Concluding, the velocities of each of the n secondary electrons are obtained as

$$v_i = v_s \frac{\hat{v}_i}{\left\|\hat{\mathbf{v}}\right\|} \quad 1 \leq i \leq n$$

where the n components $\hat{v}_i$ of vector $\hat{\mathbf{v}}$ are each sampled from a standard normal distribution.

Algorithm 2 Calculation of secondary electron emission components

$\mathscr{E}_0 \leftarrow$ energy
$\gamma_0 \leftarrow$ incident angle
$\delta_e \leftarrow \delta_{e0} \exp\left(-\frac{\mathscr{E}_0}{w_e}\right)$
$\delta_r \leftarrow$ const
$x \leftarrow \frac{\mathscr{E}_0}{\hat{\mathscr{E}}_{ts}}$
$\delta_{ts} \leftarrow \hat{\delta}_{ts} \frac{sx}{s-1+x^s}$

$R_1 \leftarrow \text{rand}(0,\ 1)$
$p \leftarrow 0$
$i \leftarrow 0$
repeat
  $n \leftarrow i$
  $P_{n,ts} \leftarrow \frac{\delta_{ts}^n}{n!} e^{-\delta_{ts}}$
  $p \leftarrow p + P_{n,ts}(1 - \delta_e - \delta_r)$
  if $n = 1$ **then**
    $p \leftarrow p + \delta_e + \delta_r$
  end if
  $i \leftarrow i + 1$
until $R_1 < p$

if $n = 0$ **then**
  absorb colliding electron
else if $n = 1$ **then**
  $R_2 \leftarrow \text{rand}(0,\ 1)$
  if $R_2 < \delta_e$ **then**
    reflect elastically colliding electron
  else if $R_2 < \delta_e + \delta_r$ **then**
    re-diffuse colliding electron
  else
    create one true secondary electron
  end if
else
  create n true secondarie electrons
end if

D. Bohm criterion

In contrast to PIC-Poisson simulations, quasi-neutral particle in cell (QPIC) simulations with a kinetic (or guiding center) description of electrons do not resolve the wall sheath structure and do not naturally force ions to flow towards the walls. Just as in the case of other quasineutral models, this must be ensured by imposing appropriate boundary conditions, namely the Bohm condition for the velocity of ions at the sheath edge.

A similar issue exists in hybrid models (kinetic ions and fluid electrons) and a review of various methods applicable to hybrid models has been recently published by Ahedo *et al.*[18] In this review, the authors have explored ways to improve the PIC weighting scheme for the density near the walls to better approximate the sharp density gradient in the neighborhood of the boundary, retaining the standard finite difference scheme to compute $E_\parallel$ from the density gradient with Boltzmann equation. The method presented below is different in essence, as it acknowledges that the sharp change of the characteristic spatial scale near the sheath edge warrants the use of a different scheme for the computation of $E_\parallel$ in the cells adjacent to the walls. Our method is in this respect more akin to the method of Lampe *et al.*[6]

Following Harrison and Thompson,[19] we first contemplate the kinetic form of the Bohm criterion for the formation of a stable plasma sheath with electrons in a Maxwell-Boltzmann equilibrium,

$$m_i \left\langle v_i^{-2} \right\rangle_w^{-1} \geq T_{e\top}, \tag{22}$$

where the brackets $\langle\,\rangle_w$ denote an average over all particles reaching the wall sheath, m_i is the ion mass, v_i the velocity of ions and $T_{e\top} = T_{e\parallel}\cos^2\alpha + T_{e\perp}\sin^2\alpha$ is the temperature in the direction perpendicular to the walls (not to the magnetic line). Note that velocity v_i in the above equation is the velocity along the field line, and not its projection in the direction normal to the walls. The reason why v_i is indeed the relevant velocity for the Bohm condition with tilted magnetic lines is discussed in Ref. 6. In principle, one should add a correction to the RHS of the above condition to account for deviations from the Maxwellian equilibrium, but this correction is neglected for the sake of simplicity.

Remembering that $E_\parallel$ is assumed constant within a cell in a cell adjacent to the sheath, one can easily extrapolate the velocity of a given ion at the walls assuming steady-state acceleration,

$$v_i^2\big|_{\zeta_w} = v_i^2\big|_{\zeta} + \frac{2eE_\parallel}{m_i}\left(\zeta_w - \zeta\right), \tag{23}$$

where ζ_w refers to the wall sheath edge position, ζ to an arbitrary position within the cell adjacent to the wall, and $E_\parallel$ to the electric field within the cell. Since Bohm's criterion is marginally fulfilled in most physical problems,[20] we shall take Eq. (22) in its exact form and combine it with Eq. (23) to obtains an implicit equation for $E_\parallel$,

$$\left\langle \frac{1}{v_i^2 + \frac{2e}{m_i}E_\parallel\left(\zeta_w - \zeta\right)} \right\rangle_{cell}^{-1} = \frac{T_{e\top}}{m_i}. \tag{24}$$

where the average is performed over the cell adjacent to the wall. The resolution of this non-linear equation at each time step would be computationally expensive, however, as it would require an iterative solver. In

order to mitigate the computational cost, we shall invoke the Schwarz inequality,[20]

$$\left\langle v_i^2 \right\rangle_w \geq \left\langle v_i^{-2} \right\rangle_w^{-1} \tag{25}$$

to derive the following criterion,

$$\left\langle v_i^2 \right\rangle_w \geq \frac{T_{e\top}}{m_i} \tag{26}$$

which matches the simplified criterion originally formulated by Bohm.[21] This means that, by satisfying the above simplified criterion in an exact form, the theoretical kinetic criterion is automatically fulfilled. With this alternative criterion (in its exact form), the equation for $E_\parallel$becomes,

$$\left\langle v_i^2 + \frac{2e}{m_i} E_\parallel \left(\zeta_w - \zeta\right) \right\rangle_{cell} = \frac{T_{e\top}}{m_i} \tag{27}$$

which has the advantage to be linear in $E_\parallel$ so that the following explicit expression can be derived,

$$E_\parallel = \frac{2}{e\left(\zeta_w - \langle\zeta\rangle_{cell}\right)} \left(T_{e\top} - \left\langle v_i^2 \right\rangle_{cell} m_i\right). \tag{28}$$

The electric field computed in boundary cells in this manner allows ions to approximately satisfy condition (26) when colliding with walls. Small departures from Eq. (26) are to be expected, however, since the calculation of $E_\parallel$ is merely an estimate which holds exactly only for a steady-state ion flow.

This technique shows some similarities with that developed by Lampe *et al.*[6] In the latter, the walls are lined with a special thin cell in which the average ion velocity is computed, after which a velocity correction is applied identically to all ions to bring their average velocity to the calculated Bohm velocity. Although similar in spirit and computational efficiency to our method, the method of Lampe *et al* lacks physical justification as no actual mechanism exists that would correct all velocities by the same amount. As in the case of our method, the kinetic Bohm criterion is substituted by a more constraining criterion, namely by the fluid Bohm criterion $\langle v_i \rangle_w^2 \geq T_{e\top}/m_i$.

1. Sheath model

It is known that, when secondary electron emission is high, a potential well may form in the close vicinity of the walls which traps part of the emitted electrons and prevents them from being re-introduced in the plasma.[22] This so-called space charge saturation is accounted for in the model by distinguishing between:

- the *well* potential, $\Phi_w \geq 0$, which is the maximum value of the potential within the sheath with respect to the wall; this is equal to zero in the absence of space charge saturation,
- the *barrier* potential, $\Phi_b > 0$, which is the maximum value of the potential within the sheath with respect to the sheath edge; in the absence of space charge saturation , the maximum potential is exactly on the wall surface and the barriers potential is simply the sheath potential (see Fig. 2).

The role of the barrier potential is to regulate the number of electrons which must reach the wall so as to compensate the net positive charge built by the absorption of ions and by the re-emission of electrons. Since

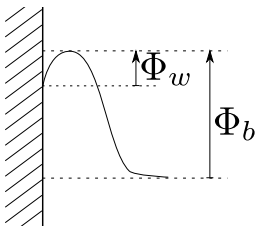

Figure 2: Schematic representation of the potential variation within the sheath in the presence of space charge saturation, showing the barrier potential Φ_b and and the well potential Φ_w.

the wall is an electrical insulator, charge conservation at the walls implies,

$$0 = j_{ew}^{+} - j_{ew}^{-} + j_{iw}, \tag{29}$$

where j_{ew}^{+} is the current density of electrons collected at the walls (coming from both the plasma bulk and the potential well), j_{ep}^{-} is the electron current density of re-emitted electrons, and j_{iw} is the collected ion current density. In principle, the barrier potential Φ_b should be adjusted at each time step to balance the ion flux and the net electron flux. In a particle-based method such as PIC, however, the statistical noise would be significant due to the low number of ions that reach the wall at each time step. This problem can be remedied by introducing some form of time-averaging procedure. Several methods have been investigated and implemented, but we shall only outline the method which was found the most robust, inspired by Taccogna *et al*.[16] The above equation is modified to form a capacitor-like equation,

$$-c_b \frac{d\Phi_b}{dt} = j_{ew}^{+} - j_{ew}^{-} + j_{iw}, \tag{30}$$

where c_b is a surface capacitance. Clearly, as $c_b \to 0$, Eq. (30) reduces to the original equation. Physically, this equation could be interpreted as the substitution of the potential barrier by a capacitor. Its interest lies in the fact that Φ_b will always change in a way that tends to counter the net charge accumulated by the wall. The value of c_b is ultimately chosen as a trade-off between low statistical noise and physical correctness.

The role of the well potential is, in turn, to regulate the emission of electrons to the plasma bulk so that the ratio j_{ew}^{-}/j_{ew}^{+} does never exceed the space charge saturated ratio derived by Hobbs and Wesson,[22]

$$\delta_{max} = 1 - 8.3\sqrt{\frac{m_e}{m_i}}. \tag{31}$$

Using a similar spirit as above, we numerically compute the well potential using the following capacitor-like equation,

$$-c_w \frac{d\Phi_w}{dt} = \left(j_{ew}^{-} - \delta_{max} j_{ew}^{+}\right) H\left(\Phi_w\right), \tag{32}$$

where $H\left(\Phi_w\right)$ is the Heaviside function, which ensures that $\Phi_w \geq 0$. This equation appropriately increases the well potential whenever the condition $j_{ew}^{-}/j_{ew}^{+} \leq \delta_{max}$ is violated. As was the case for the barrier potential, the theoretical limitation $j_{ew}^{-}/j_{ew}^{+} \leq \delta_{max}$ is asymptotically recovered as $c_w \to 0$.

III. Simulation

A. Parameters and numerical methods

Computations are performed in an axisymmetrical 1D-3V domain divided into 20 cells. Since the cells represent the discretization of a magnetic flux tube, the cross-section of each cell is inversely proportional to the field B inside the cell, which magnitude is shown in Fig. 4. The simulation is initiated with a large number of electrons and ions (typically, $N_{e0} = 20 \times 10^3$) which are assigned random energies corresponding to a Maxwellian distribution of constant temperature ($T_{e0} = 3\text{eV}$). The density of neutrals is kept constant during the simulation ($2.8 \times 10^{18}\text{m}^{-3}$ in all present simulations) and the electric field perpendicular to B is set to $E_\perp = 10\,\text{kVm}^{-1}$. The domain is bounded by walls at radii $\zeta_0 = R_0 = 3\,\text{cm}$ and $\zeta_1 = R_1 = 5\,\text{cm}$. The default parameters of the SEE model are given in Table 2.

For convenience, the geometrical domain was set up as shown on Fig. 3-b, that is, the magnetic field line is taken purely radial and the incidence of **B** on the wall is actually changed by tilting the walls appropriately. From the modeling point of view, this is roughly equivalent to the "natural" configuration shown on Fig. 3-a.

In order to analyze the influence of tilted **B**-field lines, simulations were performed for incidence angles of **B** with respect to the normal to the wall from 0° up to 80° every 20° (see Fig. 3).

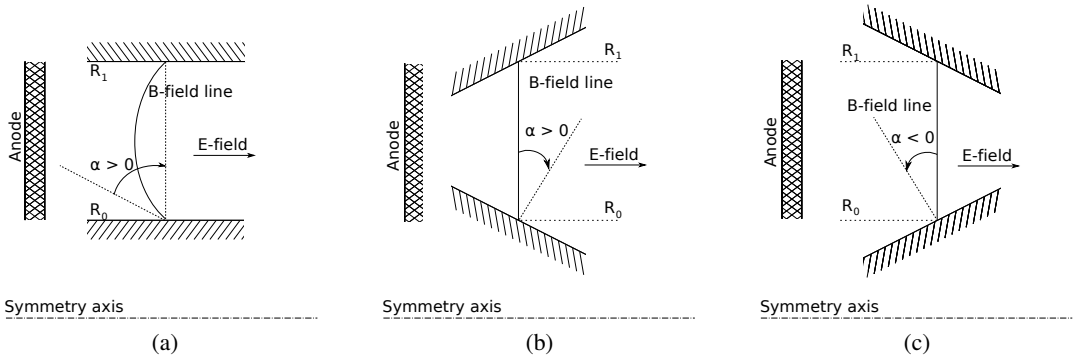

Figure 3: (a) Typical geometry of a B-field line in Hall thrusters and (b)(c) approximated problem solved in the 1D-3V simulation.

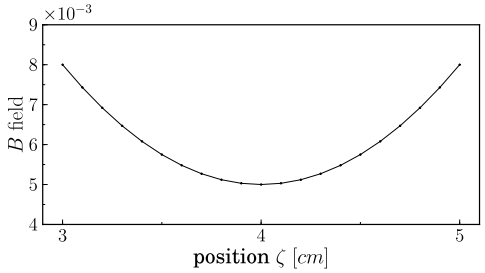

Figure 4: Magnetic field profile

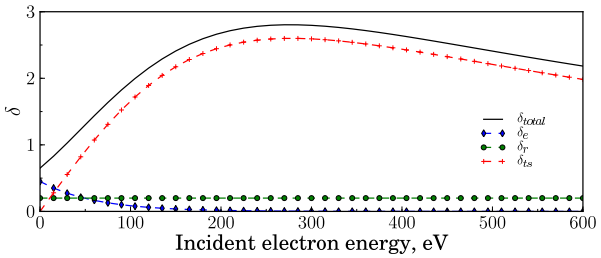

Figure 5: Components of the SEE yield and total yield.

Table 2: Default parameters of the SEE model

δ_{e0}	0.45	$\hat{\delta}_{ts}$	2.6
w_e	60	$\hat{\mathscr{E}}_{ts}$	270
δ_r	0.2	s	2

B. Simulation results

1. *Secondary electron emission influence*

In order to determine the influence of the various secondary electron emission processes, the simulation was run with angles $\alpha = 0°$and $\alpha = 60°$, using first the default SEE parameter set, later altered to account for the following cases: $\delta_e = 0$, $\delta_r = 0$ and $\delta_e = \delta_r = 0$.

It is interesting to analyze the behavior of the barrier potential in the light of the the classical sheath model in the presence of SEE,

$$e\Phi_b \backsimeq \kappa T_{e\top} \ln\left[\left(1-\bar{\delta}\right)\sqrt{\frac{m_i}{2\pi m_e}}\right], \tag{33}$$

where $\bar{\delta}$ is the total SEE coefficient averaged over the energy of impinging electrons.

With the average SEE yield from simulations reported in Table 3, *i.e.* $\bar{\delta} \approx 0.5 \div 0.8$, the above relation predicts $e\Phi_w \approx 4\kappa T_{e\top}$ which is indeed not too far off from the values reported in Table 3 with $\alpha = 0°$. Changes in δ_e and δ_r have a relatively small effect because the neglect of backscattering only contributes to the further decrease of the total SEE yield and thus to the isolation of the plasma from the walls.

The neglect of δ_e and δ_r has similarly small consequences with $\alpha = 60°$, although for this angle the sheath potential Φ_b is in all cases much smaller than could be expected from Eq. (33). The origin of this discrepancy is discussed in section 2

2. *Influence of the magnetic field lines incidence angle*

The simulation was run for several **B** field line incidence angles with the walls, using in all cases the same magnetic field profile. As shown in Fig. 11 and 12, isotropy within the channel remains more or less constant when the incidence angle is 40°, which appears to result from the relatively uniform redistribution of energy between the $\parallel$ and $\perp$ directions after collisions with the walls or the sheath.

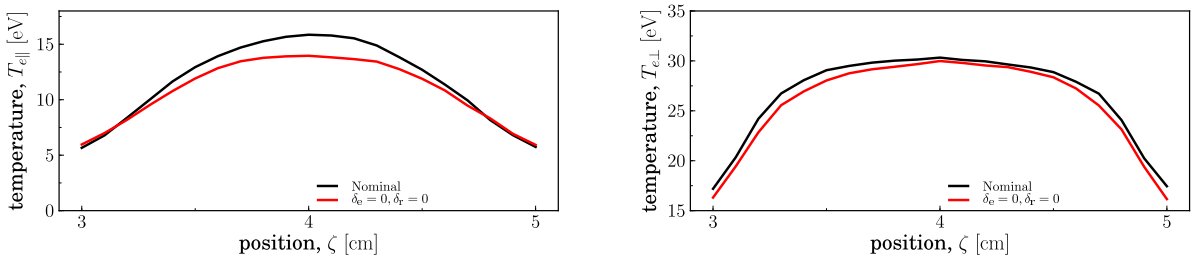

(a) $T_{e\|}$ (b) $T_{e\perp}$

Figure 6: Comparison of the electron temperature for different δ_e, δ_r with $\alpha = 60°$.

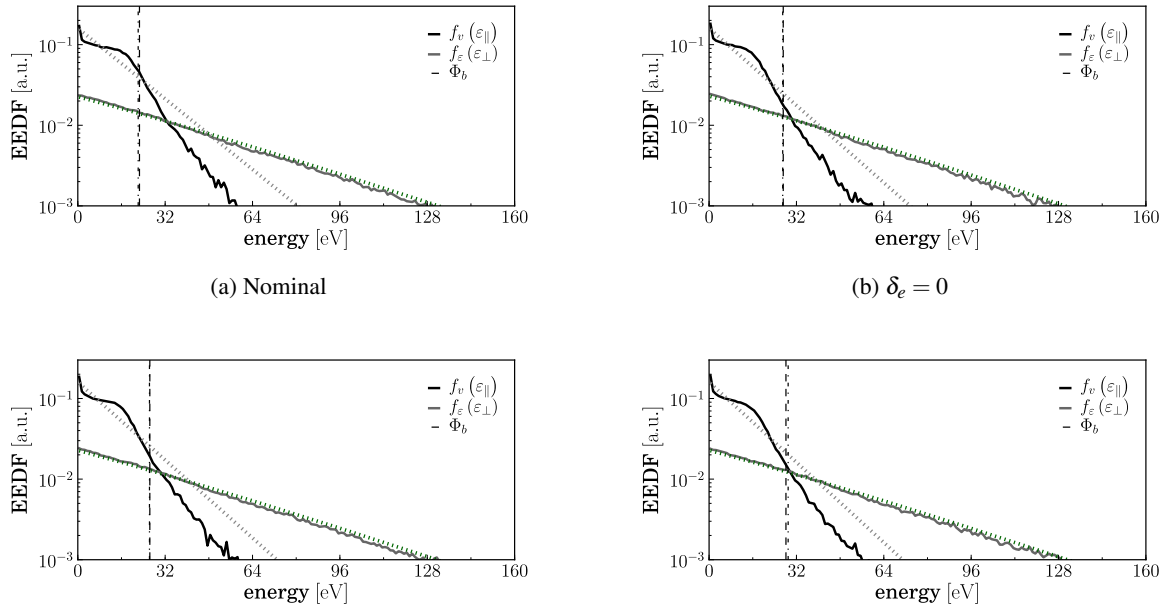

(a) Nominal (b) $\delta_e = 0$

(c) $\delta_r = 0$ (d) $\delta_e = \delta_r = 0$

Figure 7: Electron energy distribution functions for different SEE parameters with $\alpha = 60°$.

Table 3: Comparison of the time-averaged sheath properties with different SEE parameters for $\alpha = 0°$ and $\alpha = 60°$.

	$\alpha = 0°$			$\alpha = 60°$		
	Φ_b	$\bar{\delta}$	$\frac{T_{e\top}}{\Phi_b}$	Φ_b	$\bar{\delta}$	$\frac{T_{e\top}}{\Phi_b}$
Nominal	20.5	0.751	0.32	22.3	0.776	0.65
$\delta_e = 0$	20.7	0.613	0.32	27.6	0.676	0.50
$\delta_r = 0$	20.5	0.672	0.34	26.7	0.724	0.52
$\delta_e = \delta_r = 0$	21.2	0.537	0.32	29.0	0.625	0.47

It can be observed on Table 4 that the sheath potential has a non-monotonic dependence on α. As α increases from 0° to 40°, the sheath potential increases proportionally to $T_{e\top}$ as could be expected from Eq. (33). As α is increased farther, however, the sheath potential drops again and the ratio $T_{e\top}/\Phi_b$ becomes much greater than the value ≈ 0.25 suggested by Eq. (33). This peculiar behavior relates to the fact that at large $|\alpha|$, most electrons intercept the sheath edge with a grazing incidence and their energy in the direction perpendicular to the sheath is relatively low. The effective electrons temperature at the sheath edge becomes thus significantly lower than $T_{e\top}$.

A comparison was made for **B**-field lines oriented in opposite direction (see Fig. 3). Although for low angles the difference is unsignificant, for $\alpha \geq 60^\circ$ the difference in walls potential and electron temperature becomes measurable (see Fig. 13, Table 4). This is connected with the fact that electrons which intercept the sheath edge at grazing incidence are, depending on the sign of α, either close to the minimum or maximum energy of the cyclotron rotation (see Figs 3b and 3c): on one side of the magnetic flux tube, the cyclotron velocity along the drift direction is added to the drift velocity, while on the other side of the flux tube it is opposite to the drift velocity. The energy of electrons collected at the walls is accordingly higher or lower, hence the increase of SEE yield $\bar{\delta}$ as α increases from -60° to 60°.

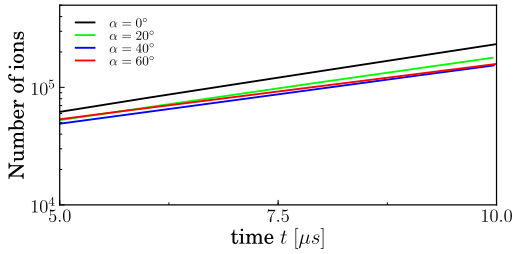

Figure 8: Evolution in time of the total number of ions ($\approx$electrons) for different values of α.

Table 4: Comparison of the time-averaged sheath properties for different values of α.

angle	Φ_b	$\bar{\delta}$	$\frac{T_{e\top}}{\Phi_b}$
$\alpha = 0^\circ$	20.5	0.751	0.32
$\alpha = 20^\circ$	29.1	0.748	0.28
$\alpha = 40^\circ$	32.9	0.756	0.33

angle	Φ_b	$\bar{\delta}$	$\frac{T_{e\top}}{\Phi_b}$
$\alpha = 60^\circ$	22.3	0.776	0.65
$\alpha = -60^\circ$	27.5	0.739	0.50
$\alpha = 80^\circ$	9.7	0.822	1.85

IV. Conclusion

A detailed model of plasma-wall interactions has been implemented in a quasineutral PIC guiding-center Hall thruster simulation. A realistic but yet manageable kinetic model of SEE is proposed, where elastic backscattering, inelastic backscattering and true secondary emission are accounted for. Boundary conditions for the guiding-center electron model at the sheath edge are derived, which approximately enforce Bohm condition and take into account the fact that the probability of collision of electrons with the sheath becomes gyrophase-dependent when magnetic lines are not perpendicular to the walls. This correlation was found to significantly affect the sheath characteristics for magnetic lines tilted from the normal to the wall by an angle equal or greater than 60°.

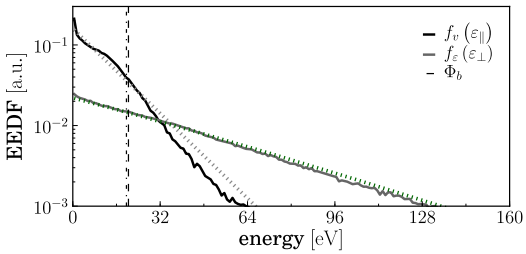

(a) $\alpha = 0°$

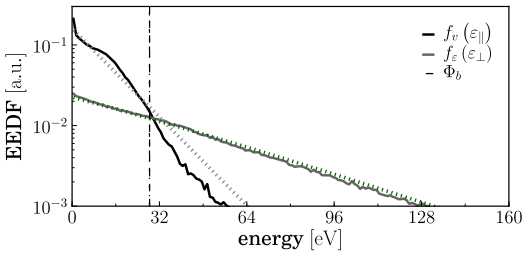

(b) $\alpha = 20°$

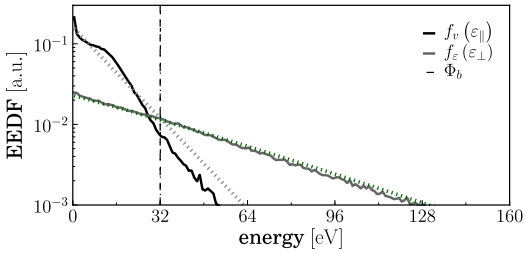

(c) $\alpha = 40°$

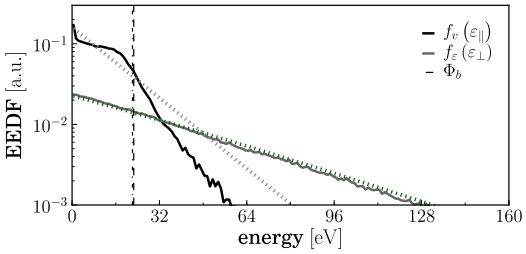

(d) $\alpha = 60°$

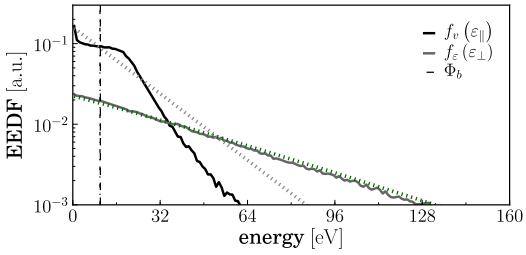

(e) $\alpha = 80°$

Figure 9: Electron energy distribution functions for different values of α.

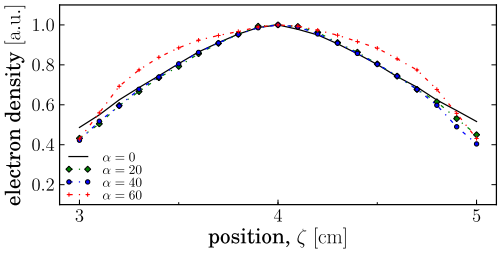

(a)

Figure 10: Comparison of normalized electrons density profiles for different values of α.

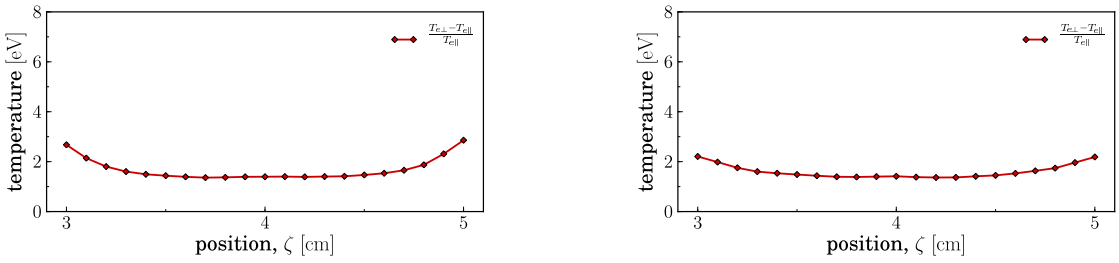

(a) $\alpha = 0°$ (b) $\alpha = 20°$

(c) $\alpha = 40°$ (d) $\alpha = 60°$

Figure 11: Relative electron anisotropy degree $\frac{T_{e\perp}-T_{e\|}}{T_{e\|}}$ for different values of α.

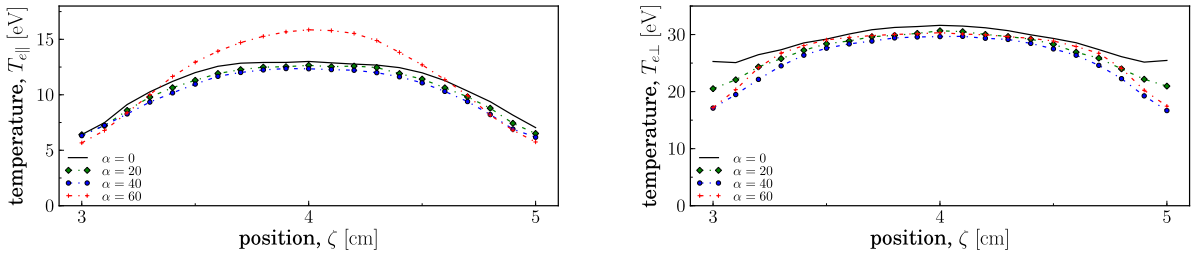

(a) $T_{e\|}$ (b) $T_{e\perp}$

Figure 12: Comparison of electron temperature for different values of α.

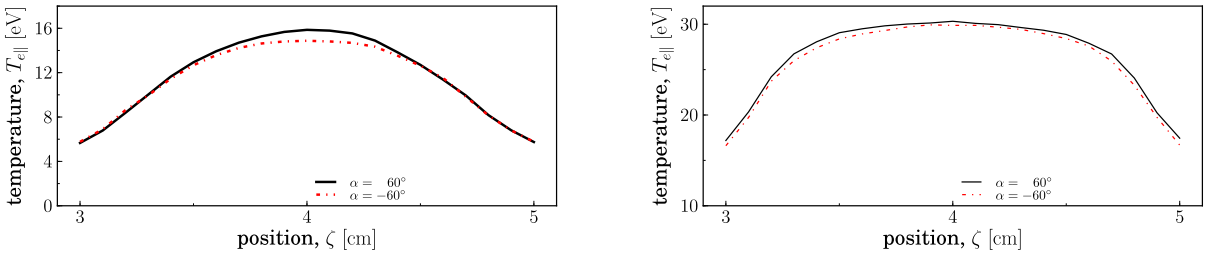

(a) $T_{e\|}$ (b) $T_{e\perp}$

Figure 13: Electron temperature for (solid black line) $\alpha = 60°$ and (dotted red line) $\alpha = -60°$.

Acknowledgment

J. Miedzik is grateful to Snecma for the sponsorship of his PhD thesis.

This work has been performed with funding from the French Research Group "Propulsion par Plasma dans l'Espace" (GDR 3161 CNRS/CNES/SNECMA/Universités).

References

[1]Keidar, M. and Boyd, I. D., "On the Magnetic Mirror Effect in Hall Thrusters," *Appl. Phys. Lett.*, Vol. 87, 2005, pp. 121501. I

[2]Choi, Y., Boyd, I. D., and Keidar, M., "Effect of a Magnetic Field in Simulating the Plume Field of an Anode Layer Hall Thruster," *J. Appl. Phys.*, Vol. 105, 2009, pp. 013303. I

[3]Ahedo, E. and Carralero, D., "Model of a Source-Driven Plasma Interacting with a Wall in an Oblique Magnetic Field," *Phys. Plasmas*, Vol. 16, 2009, pp. 043506. I

[4]Keidar, M. and Beilis, I. I., "Sheath and Boundary Conditions for Plasma Simulations of a Hall Thruster Discharge with Magnetic Lenses," *Appl. Phys. Lett.*, Vol. 94, 2009, pp. 191501. I

[5]Joyce, G., Lampe, M., and Manheimer, W. M., "Electrostatic Particle-In-Cell Simulation Technique fo Quasi-Neutral Plasma," *J. Comput. Phys.*, Vol. 138, 1997, pp. 540. I

[6]Lampe, M., Joyce, G., Manheimer, W. M., and Slinker, S. P., "Quasi-Neutral Particle Simulation of Magnetized Plasma Discharges: General Formalism and Application to ECR Discharges," *IEEE. Trans. Plasma Sci.*, Vol. 26, 1998, pp. 1592. I, A, D, D, D

[7]Miedzik, J. and Barral, S., "Electron Guiding Center Modeling for Hall Thruster Simulations," *Proc. 31st International Electric Propulsion Conference*, No. 09-069, The Electric Rocket Propulsion Society, Worthington, OH, Ann Arbor, MI, 2009. I, A

[8]Fuchs, V. and Gunn, J. P., "On the Integration of Equations of Motion for Particle-In-Cell Codes," *J. Comput. Phys.*, Vol. 214, 2006, pp. 299. A

[9]Ahedo, E., Gallardo, J. M., and Martínez-Sánchez, M., "Effects of the Radial Plasma-Wall Interaction on the Hall Thruster Discharge," *Phys. Plasmas*, Vol. 10, 2003, pp. 3397. C

[10]Barral, S., Makowski, K., Peradzyński, Z., Gascon, N., and Dudeck, M., "Wall Material Effects in Stationary Plasma Thrusters. II. Near-Wall and In-Wall Conductivity," *Phys. Plasmas*, Vol. 10, 2003, pp. 4137. C

[11]Raitses, Y., Smirnov, A., Staack, D., and Fisch, N. J., "Measurements of Secondary Electron Emission Effects in the Hall Thruster Discharge," *Phys. Plasmas*, Vol. 13, 2006, pp. 014502. C

[12]Jolivet, L. and Roussel, J.-F., "Effects of the Secondary Electron Emission on the Sheath Phenomenon in a Hall Thruster," *Proc. 3rd International Spacecraft Propulsion Conference*, Cannes (France), 2000, p. 367. C

[13]Dunaevsky, A., Raitses, Y., and Fisch, N. J., "Secondary Electron Emission from Dielectric Materials of a Hall Thruster with Segmented Electrodes," *Phys. Plasmas*, Vol. 10, 2003, pp. 2574. C

[14]Viel-Inguimbert, V., "Secondary Electron Emission of Ceramics used in the Channel of SPT," *Proc. 28th International Electric Propulsion Conference*, No. 03-258, The Electric Rocket Propulsion Society, Worthington, OH, Toulouse (France), 2003. C

[15]Furman, M. A. and Pivi, M. T. F., "Probabilistic Model for the Simulation of Secondary Electron Emission," *Phys. Rev. ST AB*, Vol. 5, 2002, pp. 124404. C, 1, 1

[16]Taccogna, F., Longo, S., and Capitelli, M., "Plasma Sheaths in Hall Discharge," *Phys. Plasmas*, Vol. 12, 2005, pp. 093506. C, 1, 1

[17]Greenwood, J., "The Correct and Incorrect Generation of a Cosine Distribution of Scattered Particles for Monte-Carlo Modelling of Vacuum Systems," *Vacuum*, Vol. 67, 2002, pp. 217. 1

[18]Ahedo, E., Santos, R., and Parra, F. I., "Fulillment of the Kinetic Bohm Criterion in a Quasineutral Particle-In-Cell Model," *Phys. Plasmas*, Vol. 17, 2010, pp. 073507. D

[19]Harrison, E. R. and Thompson, W. B., "The Low Pressure Plane Symmetric Discharge," *Proc. Phys. Soc.*, Vol. 74, No. 2, 1959, pp. 145. D

[20]Riemann, K. U., "The Bohm Criterion and Sheath Formation," *J. Phys. D: Appl. Phys.*, Vol. 24, 1991, pp. 493. D, D

[21]Bohm, D., *The Characteristics of Electrical Discharges in Magnetic Fields*, MacGraw-Hill, New York, 1949. D

[22]Hobbs, G. D. and Wesson, J. A., "Heat Flow Through a Langmir Sheath in the Presence of Electron Emission," *Plasma Phys.*, Vol. 9, 1967, pp. 85. 1, 1